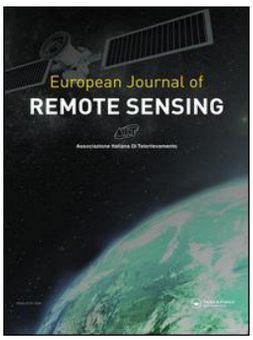

European Journal of Remote Sensing

ISSN: (Print) 2279-7254 (Online) Journal homepage: http://www.tandfonline.com/loi/tejr20

Atmospheric correction of Landsat-8/OLI and Sentinel-2/MSI data using iCOR algorithm: validation for coastal and inland waters

L. De Keukelaere, S. Sterckx, S. Adriaensen, E. Knaeps, I. Reusen, C. Giardino, M. Bresciani, P. Hunter, C. Neil, D. Van der Zande & D. Vaiciute

To cite this article: L. De Keukelaere, S. Sterckx, S. Adriaensen, E. Knaeps, I. Reusen, C. Giardino, M. Bresciani, P. Hunter, C. Neil, D. Van der Zande & D. Vaiciute (2018) Atmospheric correction of Landsat-8/OLI and Sentinel-2/MSI data using iCOR algorithm: validation for coastal and inland waters, European Journal of Remote Sensing, 51:1, 525-542, DOI: 10.1080/22797254.2018.1457937

To link to this article: https://doi.org/10.1080/22797254.2018.1457937

Published online: 16 May 2018.

EUROPEAN JOURNAL OF REMOTE SENSING, 2018
VOL. 51, NO. 1, 525–542
https://doi.org/10.1080/22797254.2018.1457937

Taylor & Francis
Taylor & Francis Group

Atmospheric correction of Landsat-8/OLI and Sentinel-2/MSI data using iCOR algorithm: validation for coastal and inland waters

L. De Keukelaere[a], S. Sterckx[a], S. Adriaensen[a], E. Knaeps[a], I. Reusen[a], C. Giardino[b], M. Bresciani[b], P. Hunter[c], C. Neil[c], D. Van der Zande[d] and D. Vaiciute[e]

[a]Remote Sensing group, Vlaams Instituut voor Technologisch Onderzoek (VITO), Mol, Belgium; [b]Optical Remote Sensing group, Consiglio Nazionale delle Ricerche – Instituto per il rilevamento elettromagnetico dell'ambiente (CNR-IREA), Milan, Italy; [c]Biological and Environmental Sciences, School of Natural Sciences, University of Stirling, Stirling, UK; [d]Operational Directorate Natural Environments, Royal Belgian Institute of Natural Sciences (RBINS), Brussels, Belgium; [e]Coastal Research and Planning Institute, Marine Science and Technology Centre, University of Klaipeda, Klaipeda, Lithuania

ABSTRACT

Image correction for atmospheric effects (iCOR) is an atmospheric correction tool that can process satellite data collected over coastal, inland or transitional waters and land. The tool is adaptable with minimal effort to hyper- or multi-spectral radiometric sensors. By using a single atmospheric correction implementation for land and water, discontinuities in reflectance within one scene are reduced. iCOR derives aerosol optical thickness from the image and allows for adjacency correction, which is SIMilarity Environmental Correction (SIMEC) over water. This paper illustrates the performance of iCOR for Landsat-8 OLI and Sentinel-2 MSI data acquired over water. An intercomparison of water leaving reflectance between iCOR and Aerosol Robotic Network – Ocean Color provided a quantitative assessment of performance and produced coefficient of determination (R^2) higher than 0.88 in all wavebands except the 865 nm band. For inland waters, the SIMEC adjacency correction improved results in the red-edge and near-infrared region in relation to optical *in situ* measurements collected during field campaigns.

ARTICLE HISTORY
Received 2 August 2017
Revised 1 March 2018
Accepted 23 March 2018

KEYWORDS
Icor; atmospheric correction; adjacency effects; SIMEC; Landsat-8 OLI; Sentinel-2 MSI

Introduction

Remote sensing has been proven useful in many terrestrial and aquatic applications such as crop monitoring, mapping of invasive species or obtaining water quality information. However, deriving reliable information from remotely sensed data is challenging as the signal detected by the sensor is subject to atmospheric influences. The scattering and absorption of molecules and aerosols present in the atmosphere modify the pure reflectance originating from the target object. Many atmospheric correction algorithms have been developed to remove these unwanted effects, however multiple correction procedures are sensor specific and either developed for land (e.g. Conel, Green, Vane, Bruegge, & Alley, 1987; Hadjimitsis et al., 2010; Kruse, 1988) or water (Gao, Montes, Davis, & Goetz, 2009; Gordon & Wang, 1994; Ioccg, 2009; Mobley, Werdell, Franz, Ahmad, & Bailey, 2016). Common methods for ocean colour atmospheric correction do not look at elevation or adjacency effects and make assumptions on reflectance in the near-infrared (NIR) (e.g. Gordon & Wang, 1994) or short-wave infrared (SWIR) (e.g. Vanhellemont & Ruddick, 2015) wavelengths. These assumptions are not valid for land targets. Land atmospheric corrections often consider a Lambertian surface, while the air-water interface has a specular reflection (Gao et al., 2009). We present an alternative atmospheric correction tool image correction for atmospheric effects (iCOR) designed to work over inland, coastal or transitional waters and land.

iCOR depends on auxillary data for the atmospheric correction. Auxiliary data can originate from external sources or be derived from the image itself and include: digital elevation model (DEM), solar and viewing angles and the atmospheric composition. The satellite overpass time, sensor and sun position provide information on solar and viewing angles. The atmospheric composition is more difficult to retrieve and consists of molecular and aerosol scattering and absorption by gases, such as water vapor, ozone and oxygen. The aerosol contribution can be described by a combination of an aerosol model (e.g. Urban, Rural, Maritime or Desert Model (Carr, 2005)) and the aerosol optical thickness (AOT). The aerosol model describes the optical properties of the aerosols, i.d. single scattering albedo, phase function, extinction and scattering coefficients (Carr, 2005). The AOT indicates how much direct sunlight is prevented from reaching the ground by these aerosol particles (van

CONTACT L. De Keukelaere liesbeth.dekeukelaere@vito.be Remote Sensing group, Vlaams Instituut voor Technologisch Onderzoek (VITO), Boeretang 200, Mol 2400, Belgium

Donkelaar et al., 2010). An important, but often neglected contributor to the TOA radiance is the adjacency effect (Richter, Bachmann, Dorigo, & Müller, 2006a; Vermote, Tanré, Deuzé, Herman, & Morcrette, 1997) which refers to light originating from neighbouring pixels and scattered into the target-sensor path. If adjacency effects are not properly considered, the overall apparent surface contrast decreases as bright pixels will be darkened and dark pixels brightened (Lyapustin & Kaufman, 2001). When atmospheric components are known or estimated, they can be imported into radiative transfer models (e.g. Moderate-Resolution Atmospheric Radiance and Transmittance Model – version 5 (MODTRAN5) (Berk et al., 2006) or Second Simulation of a Satellite Signal in the Solar Spectrum (6S) (Vermote, Tanré, Deuzé, Herman, & Morcrette, 1994)) to retrieve the surface reflectance from the TOA radiance. iCOR uses MODTRAN5 Look-Up-Tables (LUTs) to remove atmospheric effects and the implemented AOT retrieval and adjacency correction over water are supported by image-based information. The next two paragraphs will discuss both topics more in detail.

Image-based AOT retrieval algorithms typically make assumptions about dark objects in the image. These dark objects are more sensitive to atmospheric effects as the atmospheric contribution to the overall signal is higher when compared to bright targets. Over land one of the approaches is the Dark Dense Vegetation method (DDV) (Kaufman & Sendra, 1988). This method begins with the assumption that vegetation is sufficiently dark and that the ratio between bottom-of-atmosphere reflectance at different wavelengths is constant (Ouaidrari & Vermote, 1999). This method is included in the SEN2COR atmospheric correction (Müller-Wilm, 2016). Over water, a black-pixel assumption (Gordon & Wang, 1994) is often used. This assumption expects that water absorption in the NIR wavelength region is so high that reflectance detected in this spectral region is only caused by atmospheric effects. For highly turbid waters, where this assumption is violated, one can switch to an adapted SWIR variant (Vanhellemont & Ruddick, 2015; Wang, Shi, & Tang, 2011). This black pixel approach for NIR or SWIR is implemented in ACOLITE (Vanhellemont & Ruddick, 2016). In iCOR, an adapted version of the Self Contained Atmospheric Parameters Estimation from MERIS data (SCAPE-M) method, developed by Guanter (2007), is implemented. The method exploits the spectral variability within a subset, making it less dependent on the presence of DDV and it does not pose any requirements on the water composition nor its spectral characteristics. SCAPE-M has been proven successful over land on MERIS data (L. Guanter, Del Carmen González-Sanpedro, & Moreno, 2007), Chris/Proba hyperspectral data (Guanter, Alonso, & Moreno, 2005b) and for the correction of inland waters (Guanter et al., 2010). A known shortcoming of SCAPE-M is the inability to retrieve information on the aerosol type over land (Ramon & Santer, 2005; Santer, Zagolski, & Gilson, 2007).

Adjacency effects can be corrected by including spectral information on the environment of the target in the calculations. However, the extent of the environment that influences the target observation is often unknown. Alternatively, a fixed window range can be considered which is valid for a horizontally homogeneous underlying surface and produces good results for land targets (Minomura, Kuze, & Takeuchi, 2001; Richter, Schläpfer, & Müller, 2006b). In coastal or inland waters, this approach is less favourable as the sliding average will vary from typical land to typical water value (Kiselev, Bulgarelli, & Heege, 2015). Alternative methods developed to tackle the influence of adjacent light include improve contrast between ocean & land (ICOL) (Santer et al., 2007), C-Wombat-C (Brando & Dekker, 2003) or methods based on the point spread function (Kiselev et al., 2015). The adjacency correction options available in iCOR are a fixed window range for land and the SIMilarity Environmental Correction (SIMEC) method developed by Sterckx, Knaeps, Kratzer, and Ruddick (2014) for water. SIMEC estimates the background contribution iteratively by checking against the NIR similarity spectrum (Ruddick, De Cauwer, Park, & Moore, 2006).

This paper describes the methodology of iCOR, previously known as OPERA (Sterckx et al., 2015), and shows preliminary results for the Operational Land Imager (OLI) on board of Landsat-8 (L8) and the MultiSpectral Imager (MSI) onboard of Sentinel-2 (S2). Although iCOR works over land and water, the primary focus will be the validation of coastal and inland waters. As indicated by Palmer, Kutser, and Hunter (2015) the inland water community often has to choose between the coarse spatial resolution of ocean colour sensors or the sub-optimal spectral characteristics and radiometric sensitivity of land missions. L8 and S2 are both land missions, but different studies (e.g. Pahlevan & Schott, 2013; Vanhellemont & Ruddick, 2016) show their applicability for inland and coastal water quality monitoring thanks to their high spatial resolution and high signal-to-noise ratio (SNR). For validation data from the Aerosol Robotic Network – Ocean Color (AERONET-OC) of the Belgian coast and optical *in situ* measurements collected from field campaigns in multiple inland lakes (and a lagoon) across Europe are used. Specific attention will be placed on adjacency effects in inland lakes.

Methodology

Icor workflow

The overall workflow of iCOR is presented in Figure 1. This schematic can be summarised into

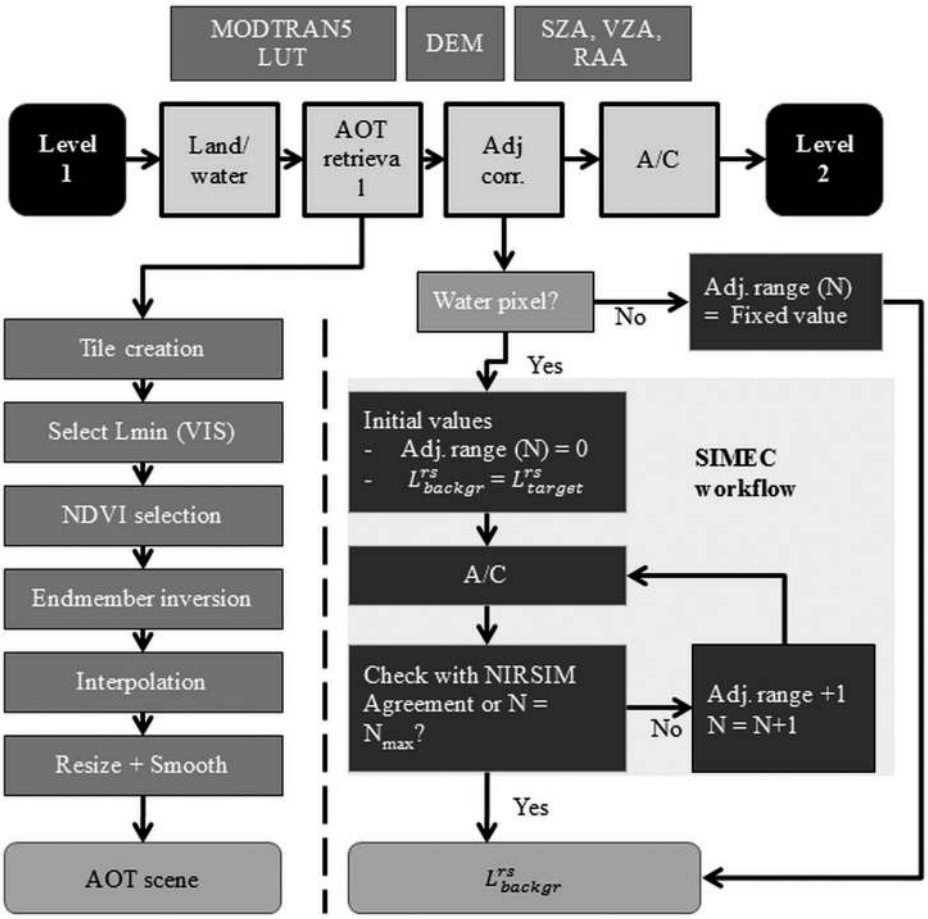

Figure 1. Workflow of iCOR atmopsheric correction from Level 1 top of atmosphere to Level 2 bottom of atmosphere product. Input parameters for the workflow are MODTRAN 5 Look-Up-Table (LUT); Digital Elevation Model (DEM); Solar Zenith Angle (SZA), View Zenith Angle (VZA) and Relative Azimuth Angle (RAA). The different modules of iCOR are: (i) land/water pixel detection, (ii) land-based AOT retrieval, (iii) adjacency correction and (iv) atmospheric correction (A/C). The subworkflows of the AOT retrieval and the adjacency correction (Adj corr.) are included.

the following steps, (i) land and water pixels are distinguished, (ii) land pixels are used to derive the AOT based on an adapted version of the method developed by Guanter (2007), (iii) an adjacency correction is performed using SIMEC (Sterckx et al., 2014) over water and fixed background ranges over land targets (Berk et al., 2006), and (iv) the radiative transfer equation is solved. iCOR uses MODTRAN5 (Berk et al., 2006) LUT to perform the atmospheric correction and uses information about the solar and viewing angles (Sun zenith angle (SZA), view zenith angle (VZA) and relative azimuth angle (RAA)) and a DEM. The next paragraphs focus on different components of the iCOR, first a small introduction on the radiative transfer function is provided, next the implemented AOT retrieval technique and the adjacency correction algorithms are described.

Radiative transfer and atmospheric correction

The radiance received by the sensor ((L^{rs}_{target}) consists of atmospheric path radiance $L_{atm-path}$ (at sensor level), background path radiance $L_{backgr-path}$ and ground reflected radiance L_{target} (Kaufman, 1984):

$$L^{rs}_{target} = L_{atm-path} + L_{backgr-path} + L_{target} \quad (1)$$

With

- $L_{atm-path}$ photon scattered into the sensor's instantaneous field-of-view, without having ground contact.
- $L_{backgr-path}$ the reflected radiation from the neighbourhood of the target pixel and diffusely scattered into the field-of-view. This term is responsible for the adjacency effect.
- L_{target} the ground reflected radiance. Over water, this component consists of the transmitted water leaving radiance and the transmitted sky glint radiance (scattered light reflecting from the surface). Sun glint is ignored.

In the atmospheric correction process, the signal is corrected for the first two terms and the surface reflectance is then retrieved from L_{target}. The three radiance components can be written as:

$$L_{atm-path} = \frac{R_{atm}(\theta_v, \theta_s, \phi_v - \phi_s)\cos\theta_s F_0}{\pi} \quad (2)$$

$$L_{backgr-path} = \frac{t_{dif}(\tau, \theta_v)\rho_{backgr} E_d}{\pi} \quad (3)$$

$$L_{target} = \frac{t_{dir}(\tau, \theta_v)\rho_s E_d}{\pi} \quad (4)$$

where F_0 is the extra-terrestrial solar irradiance, $R_{atm}(\theta_v, \theta_s, \phi_v - \phi_s)$ is a coefficient describing the reflection of light by the atmosphere, θ_s and ϕ_s are respectively the sun zenith and azimuth angle, θ_v and ϕ_v are respectively the viewing zenith and azimuth angle, E_d is downwelling irradiance just above the surface, t_{dif} and t_{dir} are respectively the diffuse and direct ground-to-sensor transmittance, τ is the optical depth in the atmosphere, ρ_s is the surface reflectance and ρ_{backgr} is the background reflectance, defined in a similar way as ρ_s. The downwelling irradiance above the surface E_d can be written as:

$$E_d = \frac{t(\theta_s)F_0\cos\theta_s}{1 - s^*\rho_{backgr}} \quad (5)$$

With $t(\theta_s)$ the total sun to surface transmittance ($t_{dir}(\tau, \theta_v) + t_{dif}(\tau, \theta_v)$) and s^* the spherical albedo of the atmosphere. Sterckx, Knaeps, and Ruddick (2011) described how to derive, starting from these equations, surface reflectance ρ_s, and derived the following equation:

$$\rho_s = \frac{c_1 + c_2 L^{rs}_{target} + c_3 L^{rs}_{backgr}}{c_4 + c_5 L^{rs}_{backgr}} \quad (6)$$

With

- $c_1 = -L_{atm-path}$
- $c_2 = 1 + \frac{t_{dif}(\tau, \theta_v)}{t_{dir}(\tau, \theta_v)}$
- $c_3 = -\frac{t_{dif}(\tau, \theta_v)}{t_{dir}(\tau, \theta_v)} = 1 - c_2$
- $c_4 = \frac{t(\theta_s)F_0\cos\theta_s t(\tau,\theta_v)}{\pi} - s^* L_{atm-path}$
- $c_5 = s^*$

Over water surfaces, an extra correction for reflected sky glint (d_1) results in the water leaving reflectance ρ_w:

$$\rho_w = \rho_s - d_1 \quad (7)$$

where

- L_{sky}

L_{sky} the downwelling sky radiance

- $r(\theta_v)$ the Fresnel reflectance

The parameters ($c_{1...5}$, d_1) depend on a large number of geometric and atmospheric parameters (solar and viewing zenith angle, ground altitude, aerosol density, water content and aerosol type) which vary over the scenes. A MODTRAN5 interrogation technique, as described in detail by De Haan and Kokke (1996), can be used to derive values for these parameters. To minimize computing time, a MODTRAN5 LUT approach is used as described in Biesemans et al. (2007). This approach assumes that the pixel is not affected by direct sun glint and that wind speed is low so that foam or white cap radiance can be ignored. Light is considered to be unpolarised and the sky radiance to be distributed in a uniform way.

Aerosol optical thickness

One of the initially unknown input parameters of the radiative transfer equation is the AOT. Various methods exist for estimating AOT, either using external sources (e.g. AERONET stations) or image-based. In iCOR we implemented an adapted version of the land based AOT retrieval technique described by Guanter et al. (2005b). The flow chart is included in Figure 1. This AOT retrieval algorithm makes use of the spectral variability of the land pixels within an image.

In a preliminary step cloud and water pixels are masked using a simple single band threshold for water and multiple thresholding levels defined for clouds (based on Guanter, Alonso, Moreno, and Member (2005a).

- The average top-of-atmosphere (TOA) reflectance for all visible and near-infrared (VNIR) bands is calculated and compared with a predefined "average" threshold. If this threshold is exceeded and the reflectance in the blue band is higher than a minimum threshold, the pixel is considered as cloud.
- For sensors with a cirrus band, an additional threshold is set on this band for the detection of cirrus clouds.

The cloud mask is dilated with an extra surrounding border to ensure that pixels affected by clouds but undetected are not considered in the AOT retrieval phase.

The raw TOA image is subdivided into tiles of about 15 × 15 km which are small enough to assume atmospheric homogeneity and large enough to include high spectral variation (Guanter et al., 2010). For each tile, the lowest radiance value within the tile is selected for each spectral band and the corresponding path radiance of this approximated dark target spectrum is retrieved using the pre-calculated MODTRAN5 LUT. The AOT value leading to the path radiance closest to the dark spectrum becomes the tile upper AOT boundary, preventing path radiance to be higher than the dark spectrum in any of the spectral bands. In the next step, the initial AOT estimation is refined through a multiparameter endmember inversion technique. Five pixels with high spectral contrast (selected

based on the NDVI values from TOA reflectance) are represented by a linear combination of two predefined default vegetation spectra and a soil spectrum (endmembers) to estimate the surface reflectance:

$$\rho_s = C_v * \rho_{veg} + C_s * \rho_{soil} \quad (8)$$

With ρ_s, ρ_{veg} and ρ_{soil} the surface reflectances of respectively the reference pixels and predefined vegetation and soil spectra. The $C_{v,s}$ parameters are left free in the inversion. This results in an 11-D inversion, with two parameters for every five pixels and AOT as degrees of freedom.

The multi-parameter endmember inversion is performed though the minimisation of the Merit function (Guanter et al., 2007):

$$\delta^2 = \sum_{1}^{N} \omega_{pix} \sum_{\lambda_i} \frac{1}{\lambda_i^2} \left[L^{SIM}_{pix,\lambda_i} - L^{SENS}_{pix,\lambda_i} \right]^2 \quad (9)$$

L^{SIM} is simulated TOA radiance, stored in and retrieved from MODTRAN5 LUT, L^{SENS} is the measured TOA radiance, λ_i is the center wavelength of the ii-th band and ω_{pix} is the weighting factor, which is 2.0 for pure vegetation, 1.5 for mixed and 1.0 for pure soil pixels to enhance the sensitivity in vegetation targets to aerosol loading. The function is weighted by λ_i^{-2} to drive the inversion towards the smaller wavelengths, where the aerosol effect is much larger than the reflectance of most natural surfaces. Minimisation of the merit function is done by the Powell's minimisation method (Press, Flannery, Teukolosky, & Vetterling, 1986).

The last step in the AOT retrieval scheme is the interpolation of missing pixels and the smoothing of the resulting mosaic. The missing data cells, deselected due to cloudiness or the land/water mask, are interpolated from neighbouring cells. To scale from cell image to per-pixel image, the cubic convolution method is used.

There are two important restrictions of this approach. Firstly, surface reflectance should be representable by a linear combination of two pure green vegetation and a bare soil endmember. Open oceans, deserts or snow landscapes do not meet this requirement. The second limitation is the difficulty in deriving a reliable estimate of aerosol model over land (Ramon and Santer (2005), Grey, North, and Los (2006)). iCOR considers a fixed rural aerosol model as default, similar as proposed by Guanter et al. (2005b) for the CHRIS/PROBA mission.

Adjacency correction

For land targets, adjacency correction assumes that environmental influences can be approximated by averaging (weighted average) the spectra of the neighbouring pixels over a fixed distance, which can be chosen arbitrarily. This weighted average spectrum can then be inserted into the radiative transfer equation as background radiance (L^{rs}_{backgr} in Equation 6). For water targets, the SIMEC adjacency correction (Sterckx et al., 2014), originally developed for hyperspectral airborne imagery (Sterckx et al., 2011), is implemented. This starts from the NIR similarity (NIR_{sim}) assumption (Ruddick et al., 2006) which states that the shape of the water spectrum in the NIR region is invariant. After normalizing the water leaving reflectance at 780 nm, the value should fall within a predefined range:

$$NIR_{sim} - Stdev \leq \frac{\rho^t_w}{\rho^r_w} \leq NIR_{sim} + Stdev \quad (10)$$

With ρ^t_w and ρ^r_w the retrieved water leaving reflectance for respectively a "test" spectral band and the "reference" spectral band situated near 780 nm. When this requirement is not fulfilled, pixels are assumed to be influenced by adjacency effects. The background radiance (L^{rs}_{backgr} in equation 6) for range N is calculated as a weighted average of the pixel radiance values surrounding the target pixel. In an iterative manner, the optimal range (N) for defining the environmental influences is determined as shown in Figure 1. Sterckx et al. (2011) defined optimal waveband settings for the "test" band as; (i) minimum influence of gaseous absorption, (ii) not lower than 690 nm because of increasing uncertainty, (iii) preferably located in the red-edge region of the spectrum where contrast between water and land is more pronounced. The availability of spectral bands is a restrictive factor in multispectral sensors. The band setting of Landsat-8 is not ideal because spectral bands at 655 nm and 865 nm are selected respectively as "test" and "reference". Sentinel-2 allows a better spectral band selection with 705 nm and 783 nm selected respectively. Sterckx et al. (2014) defined restrictions for the use of SIMEC which tends to fail in (i) high turbid waters where the NIR reflectance is flattened (Doron, Bélanger, Doxaran, & Babin, 2011; Goyens, Jamet, & Ruddick, 2013), (ii) in waters with macrophyte growth or specific algae blooms and in (iii) areas where bottom effects are significant in the NIR (optically shallow waters).

Validation in coastal and inland waters

Coastal waters

The performance of iCOR in coastal water was validated by comparing the atmospherically corrected data with AERONET-OC data. AERONET is developed by the National Aeronautics and Space Administration (NASA) to sustain atmospheric studies at various scales with worldwide autonomous sun-photometer measurements (Zibordi et al., 2009). This network has been extended in AERONET-OC to support marine applications, by providing additional capability of measuring the

radiance emerging from the sea (i.e. water-leaving radiance) with modified sun-photometers installed on offshore platforms. AERONET-OC is instrumental in satellite ocean colour validation activities through standardized measurements (i) performed at different sites with a single measuring system and protocol, (ii) calibrated with an identical reference source and method, and (iii) processed with the same code (Zibordi et al., 2009).

Two AERONET-OC stations situated in the North Sea near the Belgian coast were selected for validation; Zeebrugge-MOW1, located in coastal nearshore (3.65 km from land) waters (51.36°N, 3.12°E), and Thornton_C-Power, situated further offshore (26.25 km from land) in clearer waters (51.53° N, 2.96° E), see Figure 2. The AERONET-OC stations have a SeaWiFS Photometer Revision for Incident Surface Measurements (SeaPrism) installed, which autonomously performs multiple sky- and sea-radiance observations at programmable viewing and azimuth angles at eight (nine in the 2006 instrument release) center wavelengths in the 412–1020 nm spectral range (Zibordi et al., 2006).

Level 2.0 Quality Assured, or in absence Level 1.5 Real Time Cloud Screened, Normalized Water Leaving Radiance (Lwn) from AERONET-OC was downloaded from the AERONET website (http://aeronet.gsfc.nasa.gov/). The maximum allowed time difference between AERONET-OC measurements and the image acquisition time was set at 1 h, since water can be highly dynamic in space and time (Knaeps et al., 2015). If more than one AERONET-OC measurement fulfilled this requirement, the data were interpolated to the corresponding satellite overpass time. The validated Landsat-8 and Sentinel-2 scenes are listed in Table 1. The Lwn data [mW/(cm^2 sr um)] from AERONET-OC was converted to water leaving reflectance (ρ_w) through following formula:

$$\rho_w(\lambda) = \frac{\mathrm{Lwn}(\lambda)}{\mathrm{F0}(\lambda)} * \mathrm{pi} \quad (11)$$

With F0(λ) the exo-atmospheric solar irradiance [mW/(cm^2 sr um] at wavelength (λ) from Thuillier et al. (2003). The differences in the spectral response curves between Landsat-8, Sentinel-2 and AERONET-OC were disregarded in this analysis.

From the satellite imagery, the median ρ_w value of a 300×300 m window surrounding the AERONET-OC station was used to exclude noise coming from the station or its shadow. For Landsat-8, this resulted in an 11 × 11 window for the five bands in the VNIR. For Sentinel-2 the window was 5 × 5 pixels for B1 (443nm at 60m), 15 × 15 pixels for B5 (865 nm at 20m), and 30 × 30 pixels for B2, B3 and B4 (resp. 490, 560 and 665nm at 10m). Since the AERONET-OC stations are located at a certain distance from the coast, the effect of the surrounding land on the target pixels is assumed to be negligible and no SIMEC corrected was performed.

Inland and transitional waters

In situ data for validation of Landsat-8 and Sentinel-2 imagery were gathered during multiple field campaigns (2014–2016) in the following five European lakes: Balaton, Marken, Mantua, Garda and Geneva. Moreover field data from Curonian Lagoon was also included in the validation exercise. The location of the lakes is shown in Figure 3. An overview of the test sites is included in this paper, a full detailed description of the field campaigns can be found in Reusen et al. (2014) and Reusen et al. (2016);

- Lake Balaton is Europe's largest shallow lake at 592 km^2, located in Hungary. In spite of its large surface area, it is very shallow with a mean depth

Figure 2. True color image of port of Zeebrugge, Belgium (Landsat8 – 08/09/2014) with indication of AERONET-OC station Zeebrugge – MOW1 (51.362° N; 3.120° E) and Thornton_C Power (51.533° N; 2.955° E). © U.S. Geological Survey, USGS.

Table 1. List of data used for the validation of iCOR in coastal water. Indicated are: Date, AERONET-OC Station (Zeebrugge-MOW1 (MOW1) or Thornton_C-power (CPower)), Sensor (Landsat-8 (L8) or Sentinel-2 (S2), Scene info with Path and Row information for Landsat-8 and Orbit and Tile information for Sentinel-2, Image acquisition time, time of the first and second corresponding AERONET-OC measurement, and the Quality Level (QL) of AERONET-OC data (1.5 = Real Time Cloud Screened; 2.0 = Quality Assured).

Date	Station	Sensor	Scene info	Image time	Aeronet time 1	Aeronet time 2	Aeronet QL
01/04/2014	MOW1	L8	P199; R24	10:40:15	10:03:41	11:03:38	2.0
07/08/2014	MOW1	L8	P199; R24	10:40:03	10:28:07	10:59:37	2.0
08/09/2014	MOW1	L8	P199; R24	10:40:10	9:57:51	11:20:29	2.0
13/05/2015	CPower	L8	P200; R24	10:45:14	10:19:21	10:51:28	2.0
07/06/2015	CPower	L8	P199; R24	10:39:14	10:54:22	–	2.0
02/09/2015	CPower	L8	P200; R24	10:46:01	10:02:40	–	2.0
11/09/2015	CPower	L8	P199; R24	10:39:56	10:20:18	11:00:32	2.0
08/05/2016	CPower	L8	P199; R24	10:39:36	10:19:26	10:50:56	2.0
08/09/2016	MOW1	S2	R051; T31UES	10:50:22	10:20:34	10:50:22	1.5
27/03/2017	MOW1	S2	R051; T31UES	10:50:21	10:28:00	–	1.5
09/04/2017	MOW1	S2	R094; T31UES	10:56:51	10:23:56	–	1.5
19/04/2017	MOW1	S2	R094; T31UES	10:56:21	11:02:50	–	1.5
06/05/2017	MOW1	S2	R051; T31UES	10:50:31	11:19:01	–	1.5
09/05/2017	MOW1	S2	R094; T31UES	10:56:21	9:58:07	11:19:05	1.5
26/05/2017	MOW1	S2	R051; T31UES	10:50:31	11:19:44	–	1.5

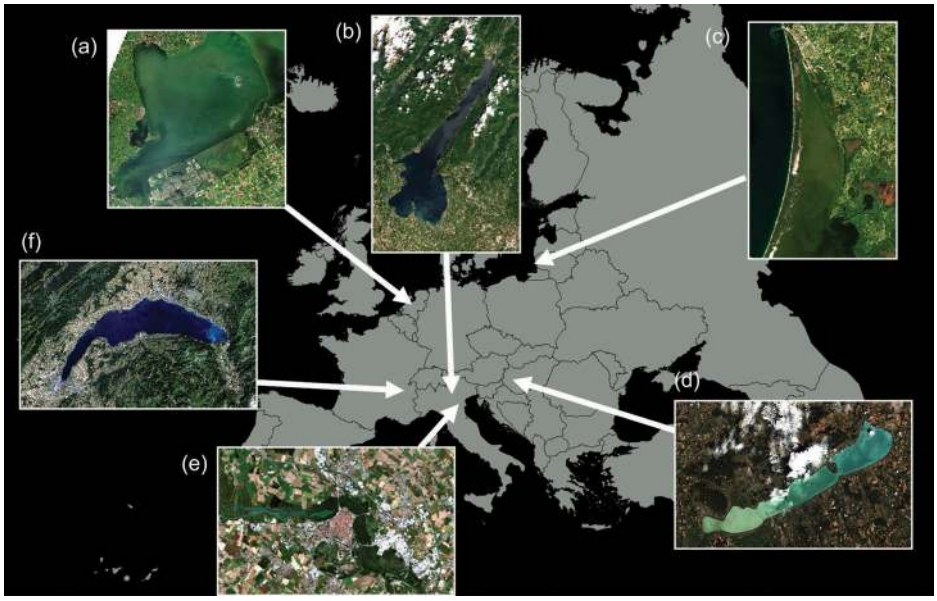

Figure 3. Location of the lakes in Europe used for validation: (a) Lake Marken (The Netherlands); (b) Lake Garda (Italy); (c) Curonian Lagoon (Lithuania); (d) Lake Balaton (Hungary); (e) Mantua Lakes (Italy); and (f) Lake Geneva (Switzerland). Note that the images are plotted not using a common geographic scale. © U.S. Geological Survey, USGS and Copernicus Sentinel data.

of approximately 3.2 m. The lake has historically been subdivided into four basins (west to east): Keszthely, Szigliget, Szemes and Siófok. The main inflow to the lake is the River Zala in the western Keszthely basin and the only outflow is via a regulated canal in the eastern Siófok basin. The trophic state of Lake Balaton varies between mesotrophic and eutrophic regimes.

- Lake Marken (Markermeer) is a 700 km^2 large, artificial, shallow, eutrophic lake in The Netherlands. It is part of a former brackish, 4000 km^2 inland sea (*Zuiderzee*) that was dammed and turned into Lake IJssel in 1932. After the construction of the *Houtribdijk* dam between the cities Lelystad and Enkhuizen, Lake Marken has been separated by sluices from the major inputs of River IJssel.
- The lakes of Mantua are composed by three small and shallow eutrophic fluvial lakes located in northern Italy. The Mantua Lakes have features typical of a shallow lentic environment due to low water velocity and limited depth, and of a wetland hosting dense macrophyte meadows, and therefore can be defined as a fluvial lake system.
- Lake Garda, located in the subalpine ecoregion of Italy has an area of 370 km^2, a water volume of 50 km^3 and a maximum depth of 346 m. From an ecological point of view, the basin can be categorised as a warm, monomictic and oligomictic basin, classified as oligo-mesotropic.
- Lake Geneva is one of the largest lakes in Western Europe with a surface area of approximately 580 km^2. The lake is extremely

deep, with a mean depth of 152 m and a maximum depth of 310 m. The main inflow into the lake is the Rhone River in the east. The lake is divided into three basins: The Upper Lake (Haut Lac) in the east receives water from the surrounding Alps via the Rhone River and as such often exhibits relatively high concentrations of mineral particles; the Large Lake (Grand Lac) is the largest and deepest basin, while the Small Lake (Petit Lac) in the south-west is shallower. Historically the lake has suffered from eutrophication, but reductions in the nutrient load have returned the lake towards an oligo-mesotrophic state – although phytoplankton blooms can occur on the lake during summer.

- Curonian Lagoon, which is the largest in Europe, is a shallow water body (total area 1584 km^2, mean depth 3.8 m) located along the south eastern coast of the Baltic Sea and geographically positioned between Lithuania and the Russian Federation. The waters are considered eutrophic or hyper-eutrophic.

Measurements of downwelling irradiance (E_d), skylight radiance (L_{sky}) and total upwelling radiance from the water (L_u) for computation of ρ_w were made using various optical radiometric devices; ASD FieldSpec FR, Satlantic HyperSAS, Trios RAMSES, Spectral Evolution or WISP-3 (Hommerson et al., 2012) and used as input in following formula (Mobley, 1999):

$$\rho_w(\lambda) = \pi \frac{L_u(\lambda) - r_{as}\ L_{sky}\ (\lambda)}{E_d(\lambda)} \qquad (12)$$

with r_{as} the air-water interface reflection coefficient. The HyperSAS and RAMSES data were processed and quality controlled using the "fingerprint" method described in Simis and Olsson (2013). *In situ* ρ_w data, collected during Landsat-8 and Sentinel-2 overpasses were compared with iCOR derived ρ_w values through scatterplots, boxplots and correlation coefficients. The list of Landsat-8 images is shown in Table 2. In total 56 matchups with Landsat-8 and 27 matchup points of Sentinel-2 were used for validation, from which the hyperspectral *in situ* reflectance data were resampled to fit the Landsat-8 and Sentinel-2 spectral response curves. The mean time difference between *in situ* measurements and image acquisition was less then 2 h.

Since inland waters can be affected by adjacency effects (e.g. Odermatt, Kiselev, Heege, Kneubühler, & Itten, 2008) two iCOR runs were performed with and without SIMEC adjacency correction, which will be referred to as the SIMEC and BASIC run respectively. In contrast to the coastal water validation, where the median value in a window of 300×300 m was selected, the inland water validation considered the average ρ_w value between the target pixel and its immediate surrounding pixels. This is to reduce the chance of including land pixels in the analysis. For Landsat-8 the mean value of a 3 × 3 pixel window was selected. For Sentinel-2, a 5 × 5 pixel window was selected for the 10 m bands, a 3 × 3 pixel window for the 20 m bands and only one pixel for the 60 m band.

Results

Coastal waters

Figure 4 shows the intercomparison between iCOR and AERONET-OC data for different bands in the VNIR regions. The four visible (VIS) bands show reasonable results with a slope varying from 0.99 to 1.17, an R^2 between 0.88 and 0.98, the root mean square error (RMSE) between 8.5e-3 and 1.4e-2 and the mean absolute percentage error (MAPE) between 13% and 65%. Band 560 nm produced the best results. Both L8 and S2 follow the same trend in these bands. The performance of the NIR band is less accurate with a slope of 2.25, and R^2 of 0.54 and RMSE of 8.9e-3. iCOR tends to overcorrect the ρ_w value in this band, which is

Table 2. List of inland lakes with the selected Landsat-8 and Sentinel-2 images and the corresponding date and number (N°) of matchups during which in-situ measurements were taken. Scene Info contains information on the Path and Row of the Landsat-8 and on Orbit and Tile of the Sentinel-2 image acquisition.

Lake	Date	Satellite	Scene info	N°
Lake Balaton, Hungary	16/07/2014	L8	P189; R027	14
	21/07/2016	L8	P189; R027	3
	22/07/2016	S2	R097; T33TXM	4
Lake Marken, Netherlands	15/09/2016	S2	R008; T31UFU	7
Mantua Lakes, Italy	23/09/2014	L8	P192; R029	6
	31/07/2015	L8	P193; R028	2
	28/07/2016	S2	R022; T32TPR	4
	19/09/2016	S2	R065; T32TPR	5
Lake Garda, Italy	22/05/2016	S2	R065; T32TPR	3
	17/08/2016	S2	R022; T32TPR	4
Lake Geneva, Switzerland	04/07/2015	L8	P196; R028	5
Curonian Lagoon, Lithuania	02/09/2014	L8	P189; R021	1
	10/06/2015	L8	P188; R021	12
	03/07/2015	L8	P189; R021	3
	04/08/2015	L8	P189; R021	10

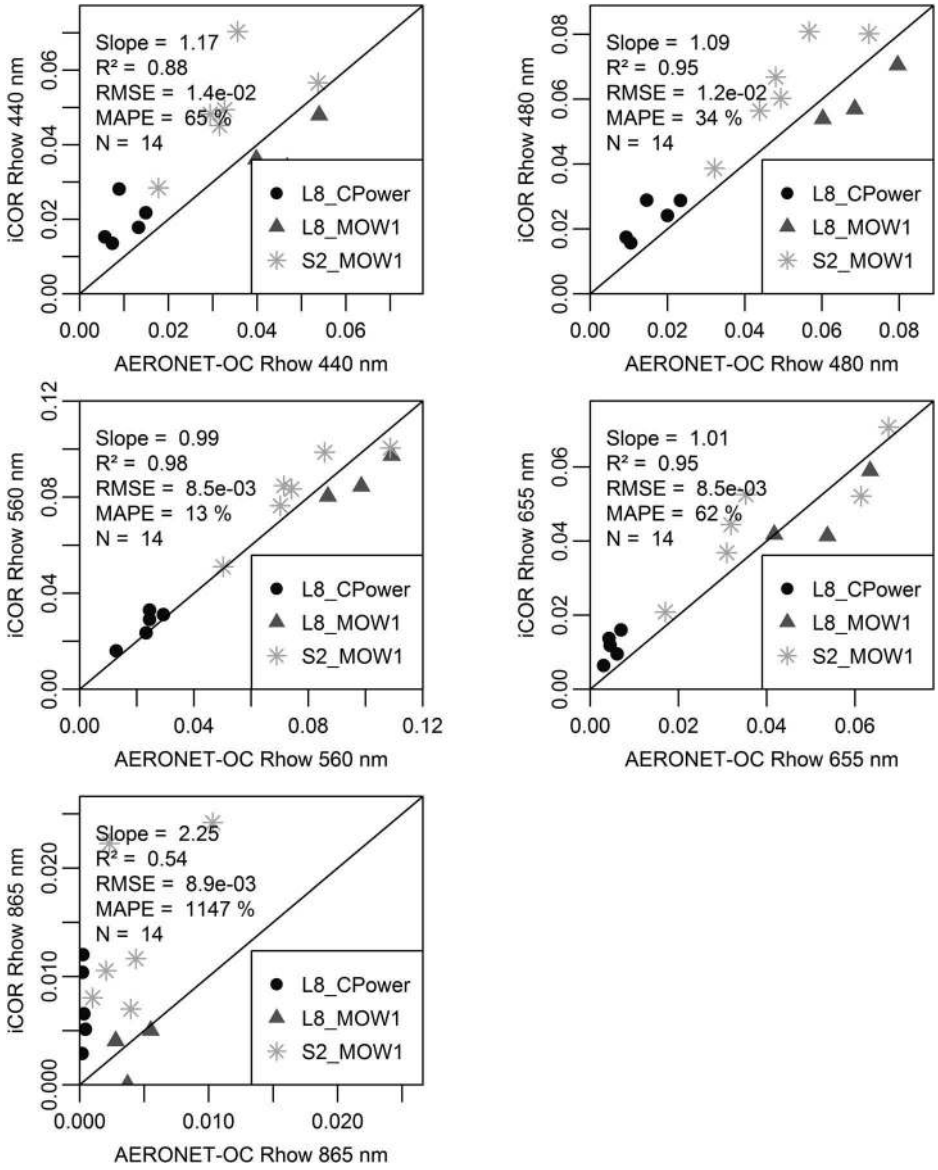

Figure 4. Scatterplots between iCOR retrieved and AERONET-OC (CPower and MOW1) water leaving reflectance (Rhow) for the five VNIR bands of Landsat-8 (440 nm, 480 nm, 560 nm, 655 nm, 865 nm) and Sentinel-2 (443 nm, 490 nm, 560 nm, 655 nm, 865 nm). The Slope, R^2, Root Mean Square Error (RMSE), Mean Absolute Percentage (MAPE) and total number of samples (N) are indicated. Black line = 1:1 line.

particularly evident at CPower station where AERONET-OC data is always lower than 4.5e-4 while iCOR ranges to 1.2e-2. The different spectral band characteristics of the sensors (neglected in this study) might explain the poorer performance at 865 nm where water absorption is high.

Inland and transitional waters

Scatterplots of iCOR ρ_w values and *in situ* collected data are shown in Figure 5 for L8 data and Figure 6 for S2 data which presents the results for the BASIC and SIMEC runs.

For Landsat-8, good agreement is demonstrated from the intercomparison exercise, especially in the VIS region where: the slope varies between 1.07 and 1.17, the R^2 value is higher than 0.87 and MAPE values are lower than 77%. The results of the 865 nm band are poorer with a slope of 2.21, R^2 of 0.6 and MAPE of 836%. Correcting for adjacency effects with SIMEC has a slightly positive effect in the VIS regions (R^2 and MAPE values remained or improved) and caused a significant amelioration in the 865 nm band: the slope dropped to 1.54, R^2 increased to 0.83 and MAPE dropped to 237%. This means that, despite the non- ideal bandsettting for Landsat-8, running SIMEC in inland waters can improve the retrieved reflectance signal.

For Sentinel-2 promising results are also retrieved in the VIS region where the slope varies between 0.8 and 0.88, R^2 is higher than 0.7 and the MAPE values are lower than 100% and with exclusion of the aerosol band (443 nm) which was lower

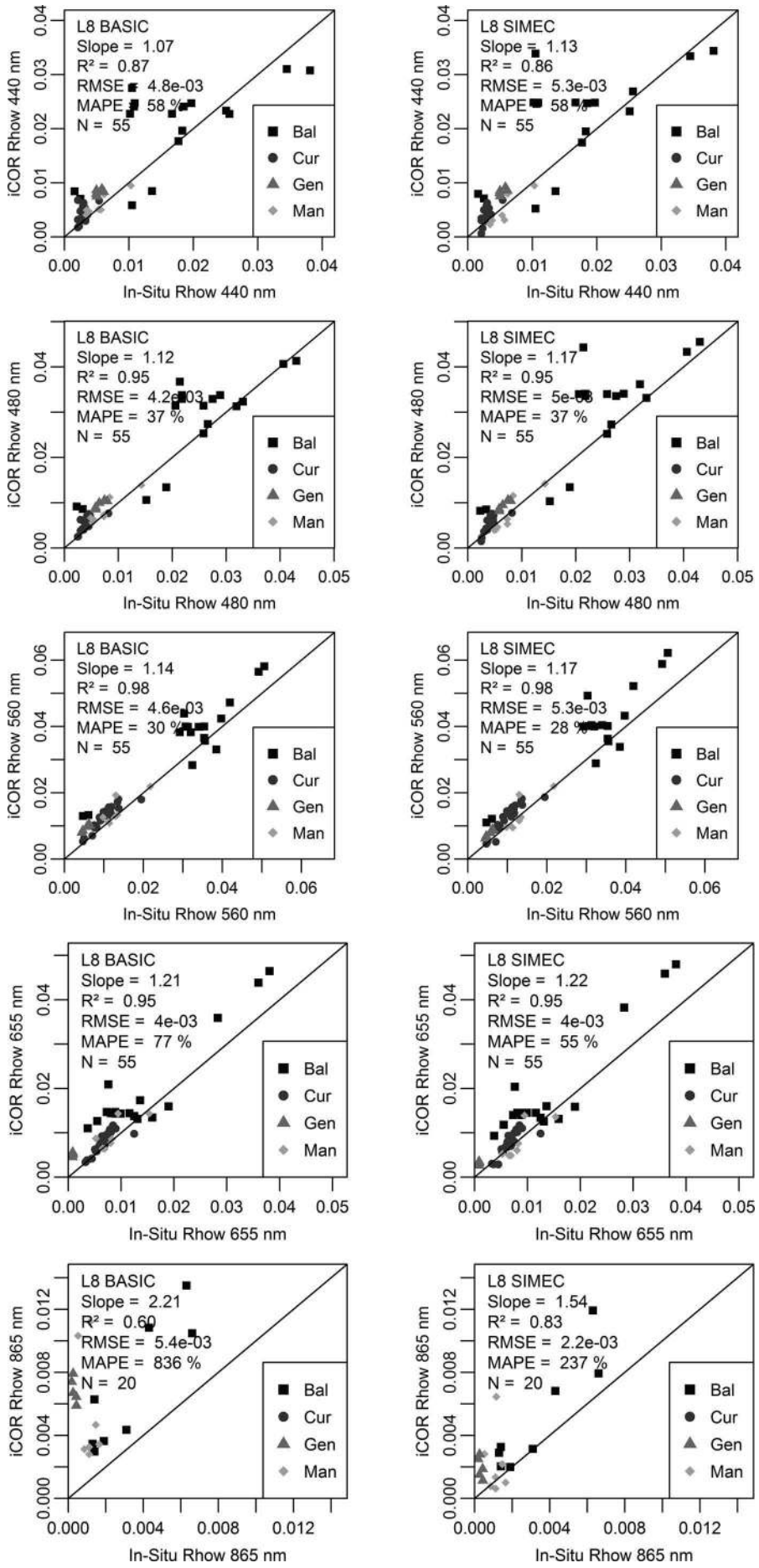

Figure 5. Scatterplots between iCOR retrieved and water leaving reflectance (Rhow) from Landsat-8 and in-situ measurements taken at four different lakes: lake Balaton (Bal), Curonian Lagoon (Cur), Lake Geneva (Gen) and Mantua lakes (Man).The left plots are the results for the basic iCOR run without SIMEC adjacency correction. The right plot shows the results when applying SIMEC. The Slope, R^2, Root Mean Square Error (RMSE), Mean Absolute Percentage (MAPE) and total number of samples (N) are indicated. Black line = 1:1 line.

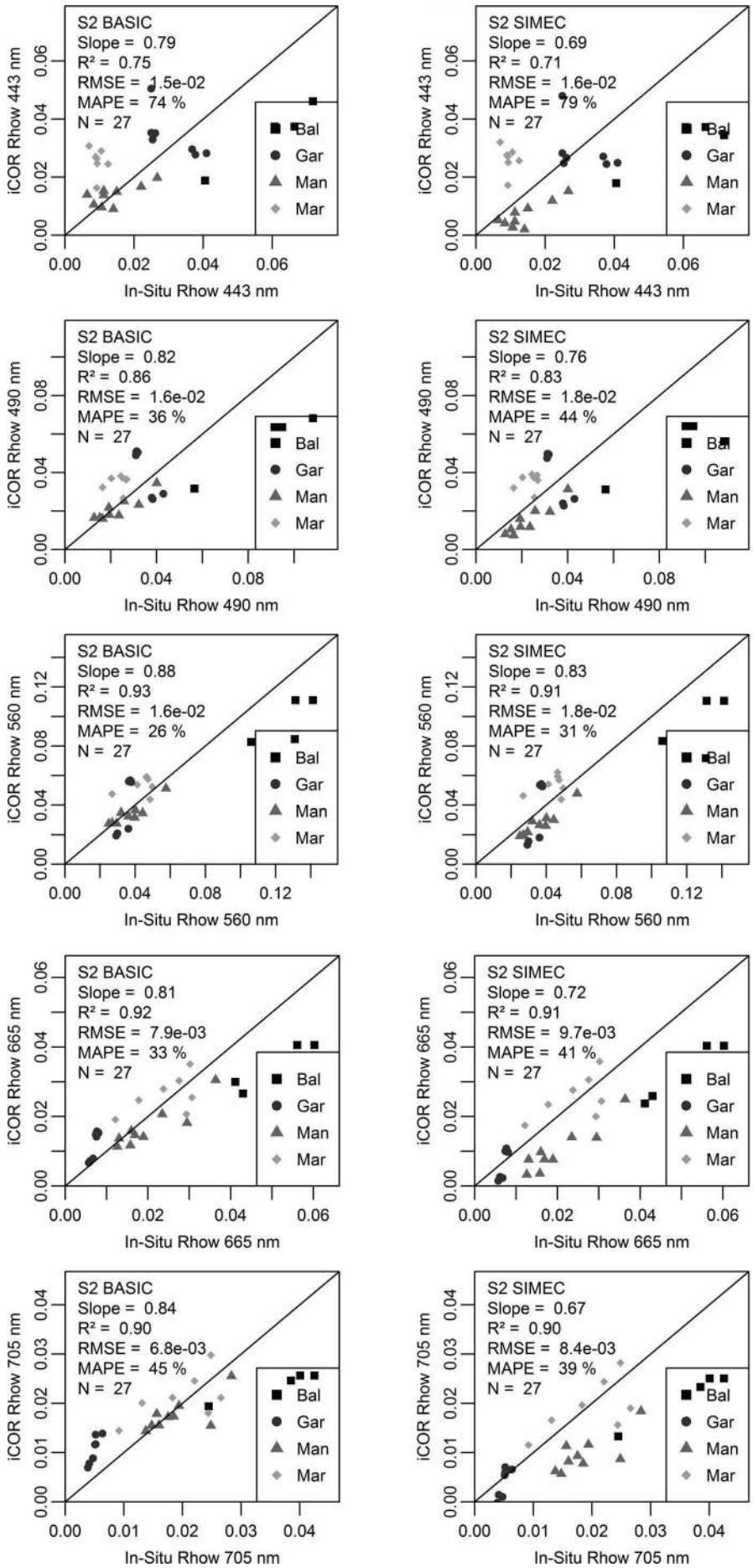

Figure 6. Scatterplots between iCOR retrieved and water leaving reflectance (Rhow) from Sentinel-2 and *in situ* measurements taken at four different lakes: lake Balaton (Bal), Lake Garda (Gar), Mantua lakes (Man) and Lake Marken (Mar). The left plots are the results for the basic iCOR run without SIMEC adjacency correction. The right plot shows the results when applying SIMEC. The Slope, R^2, Root Mean Square Error (RMSE), Mean Absolute Percentage (MAPE) and total number of samples (N) are indicated. Black line = 1:1 line.

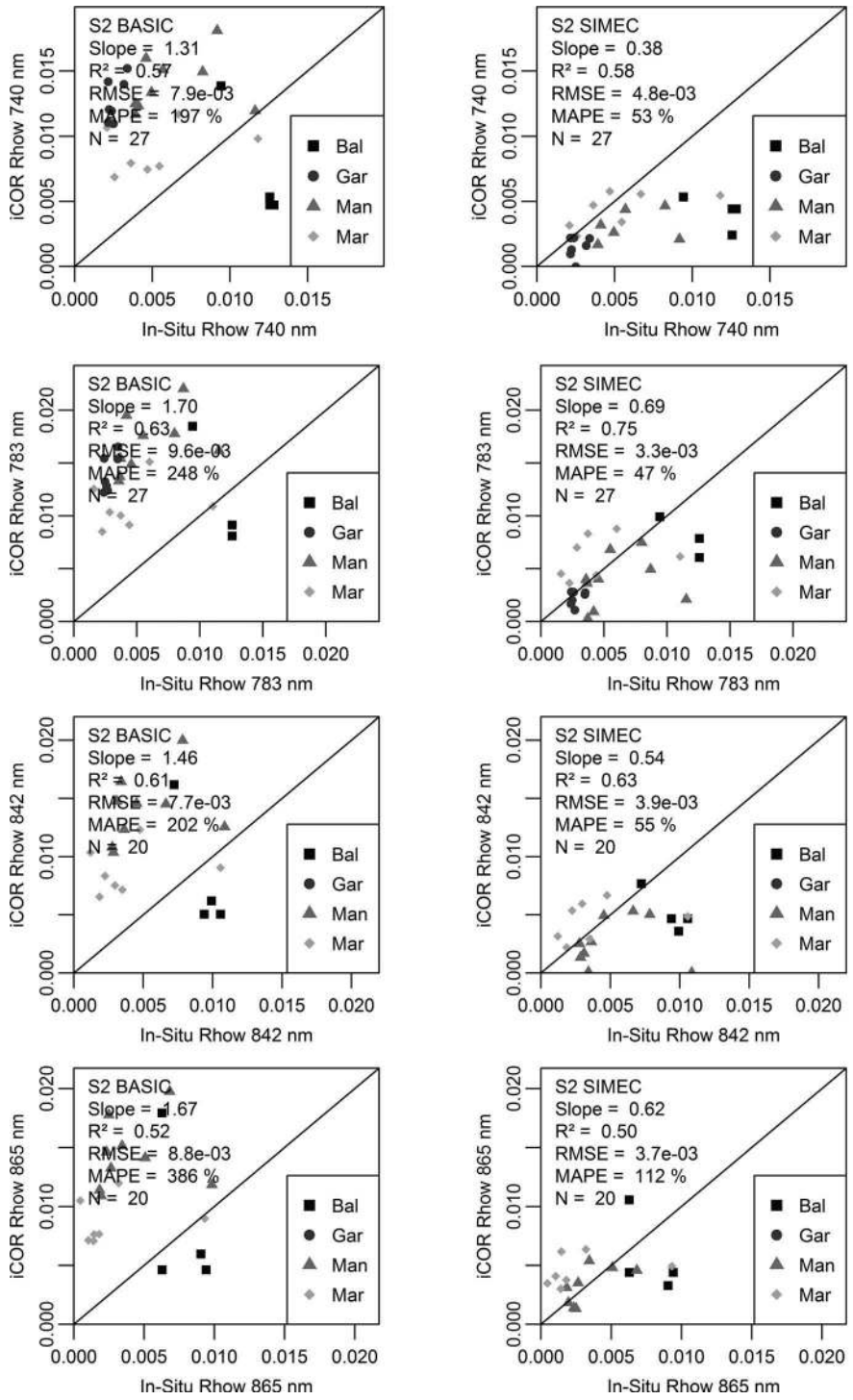

Figure 6. (continued).

than 40%. In the NIR region, the performance of the BASIC iCOR run is less satisfying with slope values high (1.31–1.7), the R^2 varying between 0.5 and 0.63 and MAPE values exceeding 100% (even 386% at 865 nm). Applying SIMEC lowered the slope in all bands. In the VIS bands this resulted is a slight deterioration of the performance with a drop in R^2 of maximum 0.1 (560 nm), RMSE increase of 0.002 and MAPE increase of up to 8%. However, from 705 nm onwards SIMEC improved the results significantly. The largest effect was noted in band 783 nm where R^2 increased from 0.63 to 0.75, the RMSE dropped from 9.6e-3 to 3.3e-3 and the MAPE value decreased from 248% to 47%.

Figure 7 shows the subtraction of *in situ* collected data from iCOR retrieved ρ_w data in boxplots. For Landsat-8, the bias is slightly lower than zero for all bands, both for the BASIC and SIMEC run. For Sentinel-2 this average approaches zero for the VIS bands in the BASIC run and are negative for the NIR bands. SIMEC seems to increase the average value,

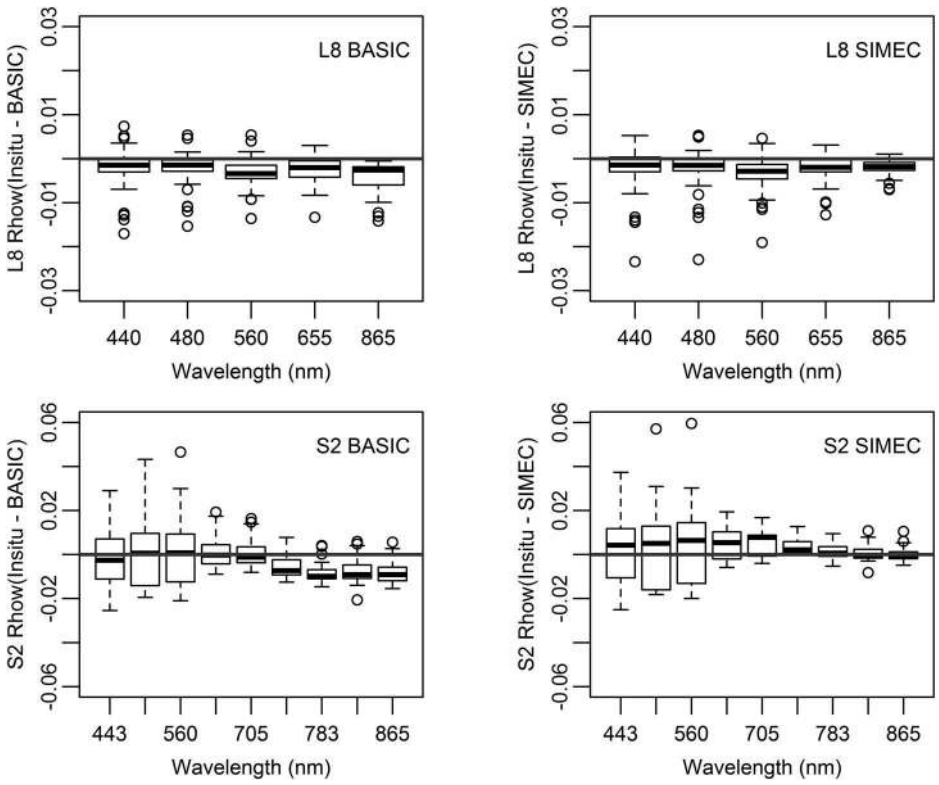

Figure 7. Boxplot of the differences between the in-situ measured spectra and the iCOR retrieved Rhow values from Landsat-8 OLI (upper) and Sentinel-2 MSI (lower) for the BASIC (left) and SIMEC (right) run.

resulting in positive values in the VIS and close to zero values in the NIR. An overcorrection by SIMEC in the VIS might be related to a slight overcorrection of the AOT or caused by the affected spectral characterisation of S2A e.g. bands B01 and B02 have been identified as being affected by a measurement defect (ESA, 2017). To better understand the effect of SIMEC on the overall spectral shape of a water pixel, Pearson Correlation coefficients between *in situ* and iCOR ρ_w values are plotted in boxplot format in Figure 8. Here it is clear that SIMEC has a positive effect on the spectral shape for both Landsat-8 and Sentinel-2 as the median Pearson correction value after SIMEC is closer to 1 and also the outliers have a higher correlation value.

The spatial extent of adjacency effects is illustrated in Figure 9 for a Landsat-8 image of Lake Mantua (23/09/2014) and in Figure 10 for a Sentinel-2 image of Lake Marken (15/09/2016). In these figures the iCOR retrieved ρ_w values at 865 nm are displayed with a colour legend. From each image three match up points are selected and their spectra (*in situ*, BASIC and SIMEC) are plotted in Figures 11 and 12 for Mantua Lakes and Lake Marken respectively.

Figure 9 shows that the reflectance in NIR without SIMEC correction is higher and the sediment plume (slightly east of Point 3) becomes more blurred. Figure 11 illustrates that the spectral shape of ρ_w is reasonably in line with the *in situ* results after

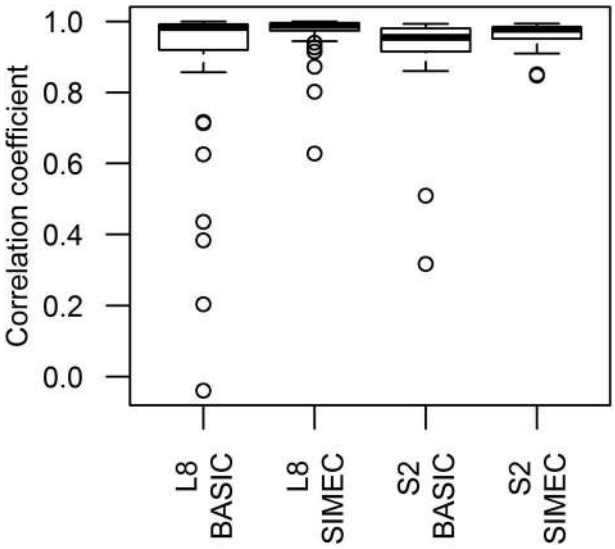

Figure 8. Boxplot of the correlation coefficients between the in-situ measured spectra and iCOR Rhow values from Landsat-8 OLI and Sentinel-2 MSI imagery for the BASIC and SIMEC run.

performing SIMEC. For Point 2 the reflectance is slightly overcorrected in the VIS. In Lake Marken, adjacency effects are especially pronounced at the border of the lake near West side.what has the highest presence of vegetation. After performing SIMEC, border effects are reduced. The spectra shown in Figure 12 indicate that SIMEC had no impact in the VIS region, but improved the results in the NIR.

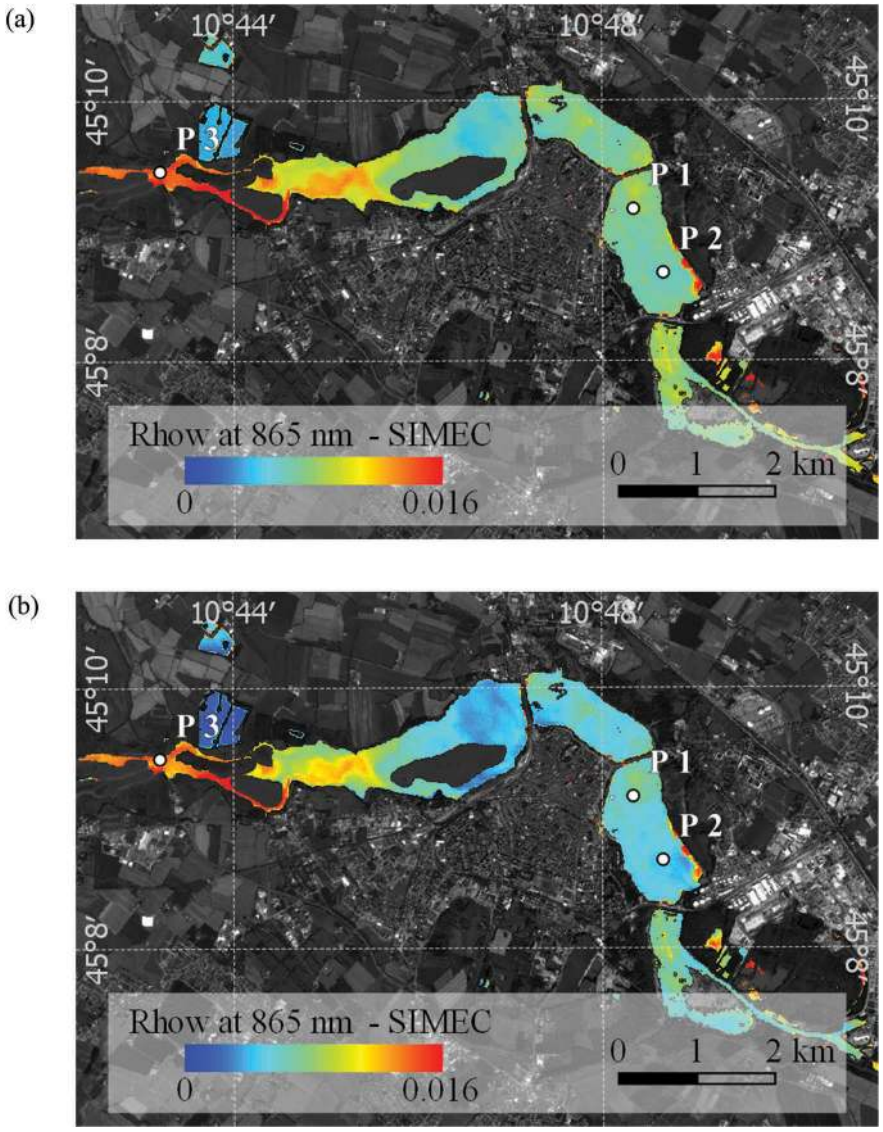

Figure 9. Water leaving reflectance at 865 nm for the Landsat-8 image of Lake Mantua (23/09/2014) without SIMEC adjacency correction (a) and with SIMEC adjacency correction (b). Three locations of insitu sampling are highlighted from which the water leaving reflectance spectra are plotted in Figure 11. © U.S. Geological Survey Landsat data, processed by VITO.

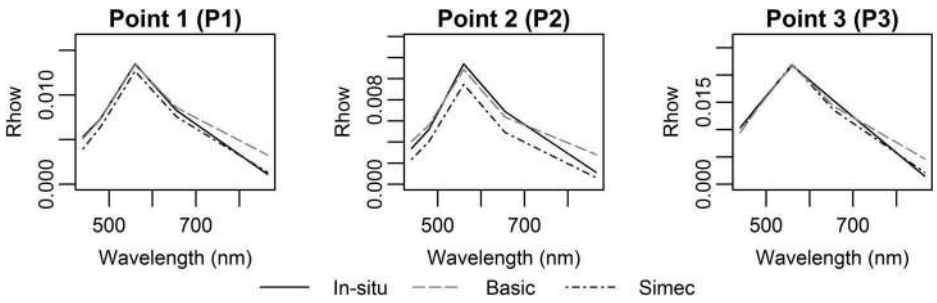

Figure 10. Water leaving reflectance at 842 nm for the Sentinel-2 image of Lake Marken (15/09/2016) without SIMEC adjacency correction (a) and with SIMEC adjacency correction (b). Three locations of in-situ sampling are highlighted from which the water leaving reflectance spectra are plotted in Figure 12. © Copernicus Sentinel data processed by VITO.

Discussion

iCOR is developed to be applicable to land and inland, transitional or coastal water scenes. The advantages and limitations of iCOR are linked to the different steps in the process.

A MODTRAN5 LUT approach solves the radiative transfer equation and takes terrain elevation and sky glint into account. However, the current version of iCOR does not correct for sun glint effects. This is an important limitation, because the viewing angles of the OLI and MSI sensor make images vulnerable to

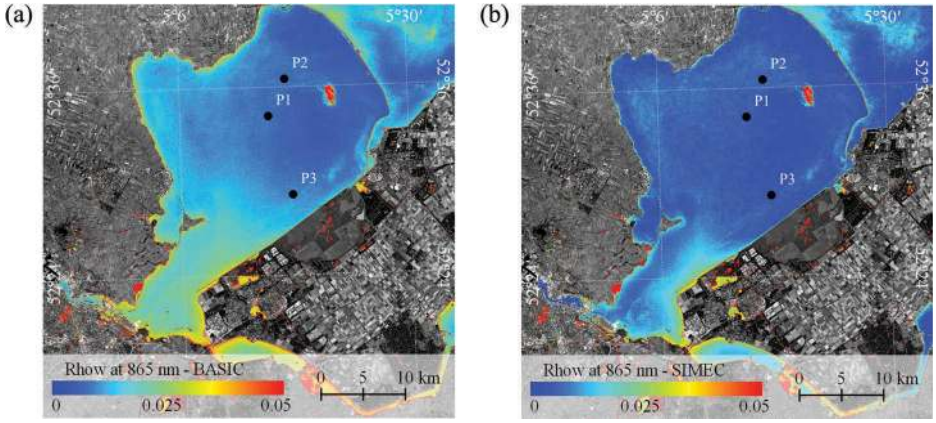

Figure 11. Water leaving reflectance at three sampling locations in Lake Mantua (23/09/2014) and the corresponding iCOR retrieved spectra from Landsat-8 with (dotdashed line) and without (dashed line) SIMEC adjacency correction. The locations of the matchups are shown in Figure 9.

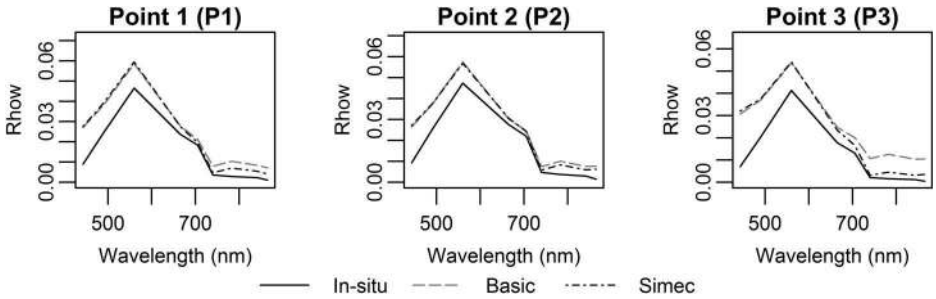

Figure 12. Water leaving reflectance at three sampling locations in Lake Marken (15/09/2016) and the corresponding iCOR retrieved spectra from Sentinel-2 with (dotdashed line) and without (dashed line) SIMEC adjacency correction. The locations of the matchups are shown in Figure 10.

sun glint contamination (Harmel, Chami, Tormos, Reynaud, & Danis, 2018). As pointed out by Kay, Hedley, and Lavender (2009) methods using statistical sea surface models, commonly used for processing of ocean colour images (e.g. Cox & Munk, 1954), are not suitable for higher resolution imaging sensors and an image-based solution is required. Removal or correction of sun glint effects will be considered in a next phase of iCOR.

With the implementation of a land-based AOT retrieval, no assumptions are made on the spectral shape of the water signal. This is a significant advantage for inland, coastal and transitional waters, since the constituents of the water are often not known and there is no dependency on SWIR bands in highly turbid waters (Knaeps, Dogliotti, Raymaekers, Ruddick, & Sterckx, 2012) which have lower SNR, especially for terrestrial missions such as L8 and S2. The main disadvantage of the current methodology is that land pixels should be present and should be representable by a linear combination of green vegetation and bare soil. When this is not the case, the user can set a default AOT value. The validation results presented in this paper show that the proximity of land allows using a continental rural aerosol model which is set as default since it is difficult to retrieve the aerosol type over land pixels (Grey et al., 2006; Ramon & Santer, 2005). In a next phase of iCOR, we will include and validate water based AOT retrieval in combination with the current land based implementation. It is expected that this will reduce errors caused by extrapolation of AOT over large water bodies.

iCOR allows the user to perform an adjacency correction over land and water. For water the SIMEC method (Sterckx et al., 2014) is implemented, which has been previously validated for MERIS data. In this paper SIMEC was validated on L8 and S2 data, and although the bandsetting of L8 was not ideal, adjacency effects were reduced after running SIMEC. But, as pointed out by Sterckx et al. (2014) some caution is needed when running SIMEC in high turbid waters, in waters with macrophyte growth or specific algae blooms or in areas where bottom effects are significant in the NIR (optically shallow waters).

In general, the assessment of iCOR for inland and coastal waters shows reasonable results for L8 and S2. The retrieved values are in line with ACOLITE results for the coastal AERONET-OC stations (Van der Zande, Vanhellemont, De Keukelaere, Knaeps, & Ruddick, 2016). iCOR results over land were tested and validated in the Atmospheric Correction Intercomparison Exercise (ACIX) organised by ESA-NASA (Doxani et al., 2018).

Conclusion

The iCOR atmospheric correction workflow is MODTRAN5 based, written in C++, and includes (i) land/water masking, (ii) land-based AOT retrieval, (iii) adjacency correction for both land (fixed ranges) and water (SIMEC) and (iv) final atmospheric correction. In this work, the iCOR performance has been tested using L8 and S2 imagery for inland, transitional and coastal waters. The validation exercise was two-fold; (i) a comparison was performed with AERONET-OC data over coastal water and (ii) with optical *in situ* data collected during dedicated field campaigns in multiple inland lakes and a lagoon around Europe. In the latter case, additional attention was paid to adjacency effects and the role of SIMEC.

Imagery acquired over the Belgian North Sea had been compared with the AERONET-OC data of Zeebrugge_MOW1, located in coastal nearshore waters, and Thornton_C-Power, further offshore in clearer waters. In these coastal waters iCOR performed well, despite the use of a fixed rural aerosol model in the atmospheric correction instead of a marine aerosol model. This was particularly true in the VIS region with an R^2 value higher than 0.88. The NIR band (865 nm) showed less accurate performance with high MAPE values and lower R^2 values. Similar trends were observed in inland lakes. The SIMEC adjacency correction showed a negligible or slightly negative effect on the ρ_w values in the VIS range (R^2 drop lower than 0.03 and RMSE increase of max 0.002), but a significant improvement in the NIR region. Here the R^2 increased with 0.23 for the 865 nm Landsat-8 band and with 0.12 for the 783 nm Sentinel-2 band. As a consequence, the overall spectral shape of the water pixels improved after running SIMEC. Also for the inland waters, band 865 nm showed the poorest results.

The iCOR atmospheric correction for L8 and S2 is freely available for users as a plugin in the SNAP Sentinel toolbox. iCOR is user-friendly and requires minimal manual interaction as the tool attempts to retrieve all required information from the image itself. Neverthess, the user is free to select various options, such as cloud or water detecting settings, or enabling the correction of adjacency effects over land and/or water.

Acknowledgments

This work was supported by the Belgian Science policy (Belspo) under Grant SR/00/003 (BELCOLOUR) and SR/00/104 (BELCOLOUR II); ESA-ESTEC under Grant 4000110059/14/NL/GLC (LVF-IMPACT) and by the European Community's Seventh Framework Programme ([FP7/2007-2013]) under Grant 606865 (INFORM) and 606797 (HIGHROC).

Disclosure statement

No potential conflict of interest was reported by the authors.

Funding

This work was supported by the European Space Agency [4000110059/14/NL/GLC];FP7 Ideas: European Research Council [606797,606865];Federaal Wetenschapsbeleid [SR/00/003,SR/00/104].

References

Berk, A., Anderson, G.P., Acharya, P.K., Bernstein, L.S., & Muratov, L. (2006). MODTRAN5: 2006 update. *Procedings of SPIE 6233, Algorithms and Technologies for Multispectral, Hyperspectral, and Ultraspectral Imagery* XII, 62331F.

Biesemans, J., Steckx, S., Knaeps, E., Vreys, K., Adriaensen, S., Hooyberghs, J., & Nieke, J., 2007, Image processing workflows for airborne remote sensing. In *5th EARSeL SIG Imaging Spectroscopy Workshop*, 23–25 April 2007, Bruges, Belgium.

Brando, V.E., & Dekker, A.G. (2003). Satellite hyperspectral remote sensing for estimating estuarine and coastal water quality. *IEEE Transactions on Geoscience and Remote Sensing*, *41*(6), 1378–1387.

Carr, S.B. (2005). The aerosol models in MODTRAN: Incorporating selected measurements from Northern Australia. *Defense Science and Technology Organisation. Australian Goverment. DSTO-TR-1803*, *1*, 1–67.

Conel, J.E., Green, R.O., Vane, G., Bruegge, C.J., & Alley, R. E. (1987). AIS-2 radiometry and a comparison of methods for the recovery of ground reflectance. In G. Vane (Ed.), *Proceedings of the 3rd Airborne Imaging Spectrometer Data Analysis Workshop JPL Publ* (Vols. 87–30, pp. 18–47). Pasadena, CA: Jet Propulsion Laboratory.

Cox, C., & Munk, W. (1954). Statistics of the sea surface derived from sun glitter. *Journal of Marine Research*, *13*, 198–227.

Doron, M., Bélanger, S., Doxaran, D., & Babin, M. (2011). Spectral variations in the near-infrared ocean reflectance. *Remote Sensing of Environment*, *115*(7), 1617–1631.

Doxani, G., Vermote, E., Roger, J., Gascon, F., Adriaensen, S., Frantz, D., & Kirches, G. (2018). Atmospheric correction inter-comparison exercise. *Remote Sensing*, *10*, 1–18.

ESA. (2017). Sentinel 2 document library - Sentinel-2 spectral response functions (S2-SRF). Retrieved December 15, 2017, from https://earth.esa.int/web/sentinel/user-guides/sentinel-2-msi/document-library/-/asset_publisher/Wk0TKajiISaR/content/sentinel-2a-spectral-responses

Gao, B.C., Montes, M.J., Davis, C.O., & Goetz, A.F.H. (2009). Atmospheric correction algorithms for hyperspectral remote sensing data of land and ocean. *Remote Sensing of Environment*, *113*(SUPPL. 1), S17–S24.

Gordon, H.R., & Wang, M. (1994). Retrieval of water-leaving radiance and aerosol optical thickness over the oceans with SeaWiFS: A preliminary algorithm. *Applied Optics*, *33*(3), 443–452.

Goyens, C., Jamet, C., & Ruddick, K.G. (2013). Spectral relationships for atmospheric correction. II. Improving NASA's standard and MUMM near infra-red modeling schemes. *Optics Express*, *21*(18), 21176–21187.

Grey, W.M.F., North, P.R.J., & Los, S.O. (2006). Computationally efficient method for retrieving aerosol optical depth from ATSR-2 and AATSR data. *Applied Optics*, *45*, 2786–2795.

Guanter, L. (2007). *New algorithms for atmospheric correction and retrieval of biophysical parameters in earth observation. Application to ENVISAT/MERIS data.* (Tesis Doctoral). València, Spain: Universitat de València.

Guanter, L., Alonso, L., & Moreno, J. (2005b). First results from the PROBA/CHRIS hyperspectral/multiangular satellite system over land and water targets. *IEEE Geoscience and Remote Sensing Letters*, *2*(3), 250–254.

Guanter, L., Alonso, L., Moreno, J., & Member, A. (2005a). A method for the surface reflectance retrieval from PROBA/CHRIS data over land: Application to ESA SPARC Campaigns. *IEEE Transactions on Geoscience and Remote Sensing, 43*(12), 2908–2917.

Guanter, L., Del Carmen González-Sanpedro, M., & Moreno, J. (2007). A method for the atmospheric correction of ENVISAT/MERIS data over land targets. *International Journal of Remote Sensing*, *28*(3–4), 709–728.

Guanter, L., Ruiz-Verdú, A., Odermatt, D., Giardino, C., Simis, S., Estellés, V., … Moreno, J. (2010). Atmospheric correction of ENVISAT/MERIS data over inland waters: Validation for European lakes. *Remote Sensing of Environment*, *114*(3), 467–480.

Haan, D., Kokke, D., & Rijkeboer. (1996). Remote sensing algorithm development Toolkit: 1. Operationalization of atmopsheric correction methods for tidal and inland waters. *BCRS Report (Netherlands: RWS-Survey Department).*

Hadjimitsis, D.G., Papadavid, G., Agapiou, A., Themistocleous, K., Hadjimitsis, M.G., Retalis, A., & Clayton, C.R.I. (2010). Atmospheric correction for satellite remotely sensed data intended for agricultural applications: Impact on vegetation indices. *Natural Hazards and Earth System Science*, *10*(1984), 89–95.

Harmel, T., Chami, M., Tormos, T., Reynaud, N., & Danis, P.A. (2018). Sunglint correction of the multi-spectral instrument (msi)-sentinel-2 imagery over inland and sea waters from swir bands. *Remote Sensing Of Environment*, *204*, 308–321.

Hommerson, A., Kratzer, S., Laanen, M., Ansko, I., Ligi, M., Bresciani, M., & Peters, S. (2012). An inter-Comparison in the field between the new Wisp-3 and other radiometers (Trios Ramses, Asd Fieldspec, and Taccs). *Journal of Applied Remote Sensing*, *6*, 063615.

Ioccg. (2009). Atmospheric correction for remotely-sensed ocean- colour products. *Reports of the International Ocean Colour Coordinating*, *10*(1998), 76.

Kaufman, Y.J. (1984). Atmopsheric effect on spatial resolution of surface imagery: Errata. *Applied Optics*, *23*(22), 4164–4172.

Kaufman, Y.J., & Sendra, C. (1988). Algorithm for automatic atmospheric corrections to visible near-IR satellite imagery. *International Journal of Remote Sensing*, *9*, 1357–1381.

Kay, S., Hedley, J., & Lavender, S. (2009). Sun glint correction of high and low spatial resolution images of aquatic scenes: A review of methods for visible and near-infrared wavelengths. *Remote Sensing*, *1*, 697–730.

Kiselev, V., Bulgarelli, B., & Heege, T. (2015). Sensor independent adjacency correction algorithm for coastal and inland water systems. *Remote Sensing of Environment*, *157*, 85–95.

Knaeps, E., Dogliotti, A.I., Raymaekers, D., Ruddick, K., & Sterckx, S. (2012). In situ evidence of non-zero reflectance in the OLCI 1020nm band for a turbid estuary. *Remote Sensing of Environment*, *120*, 133–144.

Knaeps, E., Ruddick, K.G., Doxoran, D., Dogliotti, A.I., Nechad, B., Raymaekers, D., & Sterckx, S. (2015). A SWIR based algorithm to retrieva total suspended matter in extremely turbid waters. *Remote Sensing of Environment*, *168*, 66–79.

Kruse, F.A. (1988). Use of airborne imaging spectrometer data to map minerals associated with hydrothermally altered rocks in the northern Grapevine Mountains, Nevada and California. *Remote Sensing of Environment*, *24*, 31–51.

Lyapustin, A.I., & Kaufman, Y.J. (2001). Role of adjacency effect in the remote sensing of aerosol. *Journal of Geophysical Research*, *106*, 11909–11916.

Minomura, M., Kuze, H., & Takeuchi, N. (2001). Adjacency effect in the atmospheric correction of satellite remote sensing data: Evaluation of the influence of aerosol extinction profiles. *Optical Review*, *8*(2), 133–141.

Mobley, C.D. (1999). Estimation of the remote-sensing reflectance from above-surface measurements. *Applied Optics*, *38*, 7442–7455.

Mobley, C.D., Werdell, J., Franz, B., Ahmad, Z., & Bailey, S. (2016). Atmospheric correction for satellite ocean color radiometry. *A Tutorial and Documentation NASA Ocean Biology Processing Group*, 1–73. Retrieved from https://oceancolor.gsfc.nasa.gov/docs/technical/NASA-TM-2016-217551.pdf

Müller-Wilm, U. (2016). *Sentinel-2 MSI – Level-2A prototype processor installation and user manual* (Vol 49). Retrieved from http://step.esa.int/thirdparties/sen2cor/2.2.1/S2PAD-VEGA-SUM-0001-2.2.pd

Odermatt, D., Kiselev, S., Heege, T., Kneubühler, M., & Itten, K.I. (2008). Adjacency effect considerations and air/water constituent retrieval for lake constance. *Proceedings of the '2nd MERIS | (A) ATSR User Workshop', Frascati, Italy 2008,* ESA SP-666.

Ouaidrari, H., & Vermote, E.F. (1999). Operational atmospheric correction of Landsat TM data. *Remote Sensing of Environment*, *70*(1), 4–15.

Pahlevan, N., & Schott, J.R. (2013). Leveraging EO-1 to evaluate capability of new generation of landsat sensors for coastal/inland water studies. *IEEE Journal of Selected Topics in Applied Earth Observations and Remote Sensing*, *6*(2), 360–374.

Palmer, S., Kutser, T., & Hunter, P.D. (2015). Remote sensing of inland waters: Challenges, progress and future directions. *Remote Sensing of Environment*, *157*, 1–8.

Press, W.H., Flannery, B.P.N., Teukolosky, S.A., & Vetterling, W.T. (1986). Numerical recipes: The art of scientific computing. *The mathematical Gazette, 71* (475), 245–246. ISBN 0-521-30811-9 (Cambridge University Press).

Ramon, D., & Santer, R. (2005, September 26–30). Aerosol over land with MERIS, present and future. *Proceedings of the MERIS-(A)ATSR workshop* (pp. 8). Frascati, Italy: ESA SP-597.

Reusen, I., Boenne, W., Bomans, B., De Keukelaere, L., Knaeps, E., Sterckx, S., … Vaiciute, D. (2016). *INFORM - Testing campaign report*. Retrieved from http://inform.vgt.vito.be/sites/default/files/documents/INFORM_D4.5_v1.0_withoutANNEX.pdf

Reusen, I., Knaeps, E., Hunter, P., Présing, M., Bresciani, M., Giardino, C., & Vaiciute, D. (2014). *INFORM D4.3 - Development campaign report*. Retrieved from http://inform.vgt.vito.be/sites/default/files/documents/INFORM_D4.3_v1.0.pdf

Richter, R., Bachmann, M., Dorigo, W., & Müller, A. (2006a). Influence of the adjacency effect on ground reflectance measurements. *IEEE Geoscience and Remote Sensing Letters*, *3*(4), 565–569.

Richter, R., Schläpfer, D., & Müller, A. (2006b). An automatic atmospheric correction algorithm for visible/NIR imagery. *International Journal of Remote Sensing*, *27*, 2077–2085.

Ruddick, K.G., De Cauwer, V., Park, Y.-J., & Moore, G. (2006). Seaborne measurements of near infrared water-leaving reflectance: The similarity spectrum for turbid waters. *Limnology and Oceanography*, *51*, 1167–1179.

Santer, R., Zagolski, F., & Gilson, M. (2007). Improved contrast between ocean and land (ICOL) algorithm theoretical basis document. In *Techincal report*, Version 0.1. Wimereux, France: Université du Littoral Côte d'Opale (ULCO).

Simis, S., & Olsson, J. (2013). Unattended processing of shipbone hyperspectral reflectance measurements. *Remote Sensing of Environment*, *135*, 202–212.

Sterckx, S., Knaeps, E., Adriaensen, S., Reusen, I., Keukelaere, L.D., & Hunter, P. (2015). Opera : An atmospheric correction for land and water. *Proceedings of the Sentinel-3 for Science Workshop*, (1), 3–6.

Sterckx, S., Knaeps, E., & Ruddick, K. (2011). Detection and correction of adjacency effects in hyperspectral airborne data of coastal and inland waters: The use of the near infrared similarity spectrum. *International Journal of Remote Sensing*, *32*, 6479–6505.

Sterckx, S., Knaeps, S., Kratzer, S., & Ruddick, K. (2014). SIMilarity Environment Correction (SIMEC) applied to MERIS data over inland and coastal waters. *Remote Sensing of Environment, 157,* 96-110.

Thuillier, G., Hers, M., Simon, P.C., Labs, D., Mandel, H., & Gillotay, D. (2003). Observation of the solar spectral irradiance from 200 nm to 870 nm during the ATLAS 1 and ATLAS 2 missions by the SOLSPEC spectrometer. *Metrologia*, *35*(4), 689–695.

Van der Zande, D., Vanhellemont, Q., De Keukelaere, L., Knaeps, E., & Ruddick, K. (2016, October 23–28). Validation of landsat-8/OLI for ocean colour applications with AERONET-OC sites in Belgian coastal waters. Extended abstract submitted for the 2016 Ocean optics Conference. Victoria, BC, Canada. Retrieved from: http://odnature.naturalsciences.be/downloads/publications/oceanoptics2016dimitry.pdf

van Donkelaar, A., Martin, R.V., Brauer, M., Kahn, R., Levy, R., Verduzco, C., & Villeneuve, P.J. (2010). Global estimates of ambient fine particulate matter concentrations from satellite-based aerosol optical depth: Development and application. *Environmental Health Perspectives*, *118*(6), 847–855.

Vanhellemont, Q., & Ruddick, K. (2015). Advantages of high quality SWIR bands for ocean colour processing: Examples from Landsat-8. *Remote Sensing of Environment*, *161*, 89–106.

Vanhellemont, Q., & Ruddick, K. (2016). Acolite for Sentinel-2: Aquatic applications of MSI imagery. *European Space Agency, (Special Publication) ESA SP*, *SP-740*(May), 9–13.

Vermote, E.F., Tanré, D., Deuzé, J.L., Herman, M., & Morcrette, J.J. (1994). *Second simulation of the satellite signal in the solar spectrum (6S), 6S user guide version 1, (NASA-GSFC, Greenbelt, Maryland)*. Retrieved from: http://pages.csam.montclair.edu/~chopping/EAES/6s-manual-v1.0.pdf

Vermote, E.F., Tanré, D., Deuzé, J.L., Herman, M., & Morcrette, J.J. (1997). Second simulation of the satellite signal in the solar spectrum, 6s: An overview. *IEEE Transactiosn on Geoscience and Remote Sensing*, *35*, 675–686.

Wang, M., Shi, W., & Tang, J. (2011). Water property monitoring and assessment for China's inland Lake Taihu from MODIS-aqua measurements. *Remote Sensing of Environment.*, *115*, 841–854.

Zibordi, G., Holben, B., Hooker, S.B., Mélin, F., Berthon, J.-F., Slutsker, I., … Al Mandoos, A. (2006). A network for standardized ocean color validation measurements. *Eos, Transactions American Geophysical Union*, *87*(30), 293.

Zibordi, G., Holben, B., Slutsker, I., Giles, D., D'alimonte, D., Mélin, F., … Seppälä, J. (2009). AERONET-OC: A network for the validation of ocean color primary products. *Journal of Atmospheric and Oceanic Technology*, *26*(8), 1634–1651.